Exceptional points of degeneracy and $\mathcal{PT}$ symmetry in photonic coupled chains of scatterers

Mohamed A. K. Othman,[1] Vincenzo Galdi,[2] and Filippo Capolino[1]
[1]*Department of Electrical Engineering and Computer Science, University of California, Irvine, Irvine, California 92697, USA*
[2]*Waves Group, Department of Engineering, University of Sannio, I-82100 Benevento, Italy*
(Received 11 October 2016; revised manuscript received 7 February 2017; published 17 March 2017)

We demonstrate the existence of exceptional points of degeneracy (EPDs) of periodic eigenstates in non-Hermitian coupled chains of dipolar scatterers. Guided modes supported by these structures can exhibit an EPD in their dispersion diagram at which two or more Bloch eigenstates coalesce, in both their eigenvectors and eigenvalues. We show the emergence of a second-order modal EPD associated with the parity-time ($\mathcal{PT}$) symmetry condition, at which each particle pair in the double chain exhibits balanced gain and loss. Furthermore, we also demonstrate a fourth-order EPD occurring at the band edge. Such a degeneracy condition was previously referred to as a *degenerate band edge* in lossless anisotropic photonic crystals. Here, we rigorously show it under the occurrence of gain and loss balance for a discrete guiding system. We identify a more general regime of gain and loss balance showing that $\mathcal{PT}$ symmetry is not necessary to attain EPDs. Moreover, we investigate the degree of detuning of the EPD when the geometrical symmetry or balanced condition is broken. Furthermore, we demonstrate a realistic implementation of the EPD in a coupled chain made of pairs of plasmonic nanospheres and active core-shell nanospheres at optical frequencies. These findings open avenues toward superior light localization and transport with application to high-Q resonators utilized in sensors, filters, low-threshold switching and lasing.

DOI: 10.1103/PhysRevB.95.104305

I. INTRODUCTION

Degeneracy in the state space of a dynamical system refers to points at which two or more physical eigenstates coalesce into one. This pervasive concept may give rise to interesting phenomena in many branches of physics [1–7]. In connection with electromagnetic (EM) waves, of particular interest for this study, it is well known that the propagation in closed guiding structures, such as metallic wave guides or periodic structures, in the absence of energy dissipation or gain, is mathematically described in terms of a Hermitian operator [8]. This implies that the associated eigenspace is characterized by real-valued eigenvalues and it always constitutes a basis. As a consequence, with a few notable exceptions, strict modal degeneracy cannot take place, in the sense that eigenmodes associated with identical eigenvalues are generally linearly independent. However, certain degenerate conditions can be found for which the system space is constructed from a generalized basis of eigenstates [1–3]. Simple examples of these degeneracies can be found in metallic wave guides at the cutoff or zero frequency. Another interesting example can be found at the transmission band edge of any periodic guiding structure, where there exists a regular band edge (RBE) at which forward and backward Bloch modes coalesce [9]. More pronounced degeneracy conditions, entailing the coalescence of three, four, or more Bloch modes, can be found in special classes of anisotropic or birefringent photonic crystals. An example of a third-order degeneracy is found at the stationary inflection point (SIP) of a magnetic photonic crystal (MPhC) [10,11], whereas a fourth-order degeneracy is realized at a degenerate band edge (DBE) [12–17]. At such points of degeneracy, the group velocity vanishes and the local density of states exhibits a dramatic enhancement. These effects have been demonstrated in lossless structures under RBE, SIP, or DBE conditions [9,10,12,16]. In particular, the frozen-wave regime associated with the DBE condition [5,12,16,18–22] has been demonstrated to provide a better localization of light through large enhancement of the local density of states, as well as enhancement of gain in active configurations [16,22]. Moreover, several DBE implementations have been carried out in coupled silicon wave guides [15,21] or two-dimensional (2D) photonic crystals [23], with potential applications to lasers [14,16], and more recently at microwaves [24], for low-threshold oscillations [25–27] and efficient high power generation [22,25,28].

Recently, there has been a surge of interest in connection with degeneracies in systems described by non-Hermitian operators. In these cases, the term exceptional point is used to indicate a non-Hermitian degeneracy where two or more eigenstates coalesce into one with the same complex-valued eigenvalue. Since the term "exceptional" may have different meanings in different disciplines, in what follows, we prefer to use the term "exceptional point of degeneracy" (EPD) so as to avoid possible ambiguities. The interest in this class of degeneracies is mainly motivated by their relevance in the study of parity-time- ($\mathcal{PT}$-) symmetric systems [2,3,29,30]. Originally introduced in quantum mechanics, as an alternative condition to ensure real-valued eigenspectra in the presence of pseudo-Hermitian [31–33] and non-Hermitian Hamiltonians, the $\mathcal{PT}$ symmetry concept has stimulated discussions in several branches of applied physics, including quantum field theories and quantum interactions [2,3,34,35]. Moreover, given the formal analogy with quantum mechanics, $\mathcal{PT}$ symmetry has naturally been translated to paraxial optics [29,30,36,37]. In this case, practical implementations involve coupled wave guides and resonators exhibiting symmetric gain and loss distributions with suitable spatial modulation [30,37,38], although related effects were also demonstrated in passive lossy structures [39]. Aside from the interplay between gain and loss in $\mathcal{PT}$-symmetric coupled-mode structures (see [30,40–42]), it is important to note that $\mathcal{PT}$ symmetry is not a sufficient condition for a real-valued eigenspectrum.

In fact, for non-Hermiticity (i.e., gain-loss) levels beyond a critical threshold, the system may encounter an EPD, thereby undergoing a phase transition to a complex-valued eigenspectrum. This phenomenon is usually referred to as spontaneous symmetry breaking [29,30,38]. In view of the comparatively simpler (with respect to quantum physics) implementations, optical $\mathcal{PT}$-symmetric structures have elicited a great deal of attention, leading to many interesting observations, including the demonstration of low-threshold lasing and laser absorbers [41,43–45], enhanced nonlinear effects [34,40–43,46,47], as well as metamaterial-based field manipulations [38,48,49]. In previous papers, $\mathcal{PT}$ symmetry has been shown in discrete arrangements of resonators and also using the so-called tight-binding (TB) approach [48,50]. Moreover, EPDs have been also observed in 2D and three-dimensional (3D) geometries [7,37,51].

In this paper, we study the emergence of EPDs in coupled chains of photonic scatterers exhibiting gain and loss. This configuration may constitute an interesting, and largely unexplored, photonic testbed for studying the properties of non-Hermitian systems. Moreover, it may find intriguing applications to light localization and transport.

Accordingly, the rest of the paper is laid out as follows. In Sec. II, we outline the problem statement. In Sec. III, we introduce the model utilized for the eigenmode analysis. In Sec. IV, we study the modal dispersion characteristics near second- and fourth-order EPDs, and elucidate the connections with the $\mathcal{PT}$ symmetry concept. In Sec. V, we illustrate a realistic implementation example. Finally, in Sec. VI, we provide some brief conclusions and discuss the implications and possible applications of our results.

II. PROBLEM STATEMENT

As previously mentioned, we investigate the emergence of EPDs in coupled periodic chains of polarizable particles (see Fig. 1) exhibiting loss and gain. In particular, we derive a general (necessary and sufficient) condition for an EPD to occur, and we elucidate possible connections with the $\mathcal{PT}$ symmetry concept [29,30,39].

Our paper yields two main results. First, we demonstrate the existence of EPDs by using a TB-based method. Such an approach, based on the transfer-matrix method, is conventionally utilized in the study of photonic crystal wave guides [52,53] and has been previously employed to investigate the properties of nonlinear magnetic resonators [48], discrete $\mathcal{PT}$-symmetric scatterers [50], and solitons in paired chains of dimers [50,51]. Second, we show the manifestation of both second- and fourth-order EPDs in such structures. Importantly, we demonstrate that DBEs (special kinds of EPDs) may exist in chains of discrete scatterers exhibiting loss and gain. We also elucidate the connection between these EPDs and the previously observed DBE effects in lossless structures. This paper exhibits several differences with respect to previous papers in the topical literature: By comparison with previous papers on chains of split rings [48], we emphasize that our proposed chain here is periodic along the z direction, and we find degeneracies of different orders. Furthermore, although there are some previous papers of fourth-order EPDs in chains of multiple-resonators [6,54], here, we attain these effects in a photonic chain, composed of pairs of coupled scatterers (i.e., two coupled linear chains). Moreover, we also discuss some aspects that have been insofar overlooked, including the order of degeneracies, their relationship with DBE conditions explored in a very different contest [12,23], and the associated perturbation analyses. The evolution of the eigenstate vectors in the system, to be investigated thoroughly in Sec. IV, is illustrated schematically in Figs. 2(a) and 2(b) in the vicinity of second- and fourth-order EPDs, respectively. In this paper, we will quantify the evolution of the complex Bloch wave numbers in terms of frequency detuning and the gain-loss level, which will be rigorously defined in Secs. III and IV.

We highlight that $\mathcal{PT}$ symmetry, also explored in our paper, is a particular topology (and not the only one) available to realize a gain and loss balance scheme and construct real eigenspectra. Nevertheless, as shown hereafter, it is not a necessary condition for the existence of an EPD. In principle, polarizabilities with gain can be implemented in dielectric or plasmonic nanoparticles, with gain provided by fluorescent quantum dots cores [55] or dyes in the core or in the outer shell [56] (see, e.g., the example in Sec. V). We assume

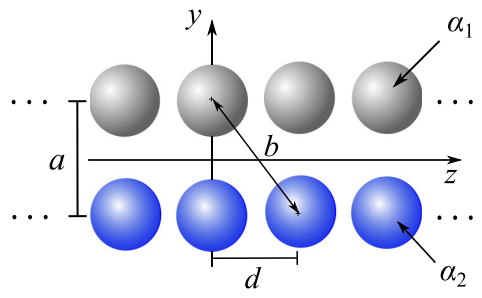

FIG. 1. Two coupled chains of polarizable particles with electrical dipolar polarizabilities α_1 and α_2. Bloch modes polarized along the x direction and propagating along the z direction are investigated. The dispersion diagram of such modes may develop an EPD under certain conditions.

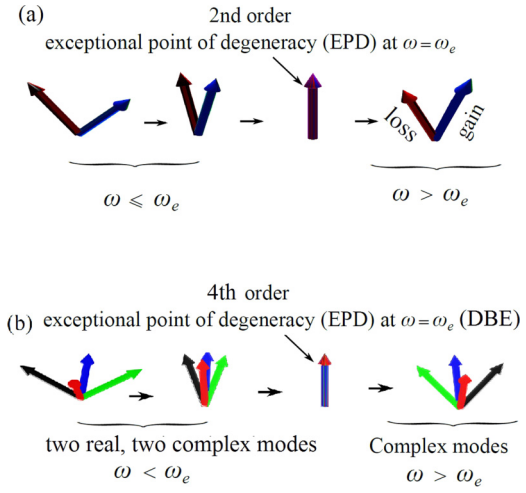

FIG. 2. Schematic representation (in 3D space) of the 4D system state eigenvectors Ψ_l near an EPD. (a) Two eigenvectors coalesce at a second-order EPD. (b) Four eigenvectors coalesce at a fourth-order EPD (DBE).

time-harmonic fields of the form $e^{-i\omega t}$, so that gain and loss correspond to complex-valued polarizabilities $\alpha = \alpha' + i\alpha''$, with $\alpha'' < 0$ and $\alpha'' > 0$, respectively.

III. EIGENMODES IN TWO COUPLED CHAINS: TRANSFER MATRIX ANALYSIS

Referring to the schematic in Fig. 1, we consider a periodic chain of dipolar scatterer pairs in a homogenous medium. Each pair is characterized by two dipole moments, with electric dipolar polarizabilities denoted by α_1 and α_2, separated by a distance a, and the chain's period is denoted by d. Accordingly, the chain's constitutive scatterers are located at $\mathbf{r}_{1,n} = (a/2)\hat{\mathbf{y}} + nd\hat{\mathbf{z}}$ and $\mathbf{r}_{2,n} = -(a/2)\hat{\mathbf{y}} + nd\hat{\mathbf{z}}$, respectively, with n denoting an integer $n \in (-\infty,\infty)$. Here and henceforth, boldface symbols denote vector quantities and the caret denotes unit vectors. The polarizabilities relate the local electric field at the equivalent electric dipoles' locations to their moment, viz. $\mathbf{p}_{j,n} = \alpha_j \mathbf{E}^{\rm loc}_{j,n}$, with $j = 1,2$. The local electric field $\mathbf{E}^{\rm loc}_{j,n}$ at $\mathbf{r}_{j,n}$ is produced by the infinite chain's dipole moments, in addition to any external excitation $\mathbf{E}^{\rm ext}_{j,n}$, through the dyadic Green's function (GF) as

$$\mathbf{E}^{\rm loc}_{j,n} = \mathbf{E}^{\rm ext}_{j,n} + \sum_{\substack{p=1\\ p\neq j}}^{2} \sum_{\substack{q=-\infty,\\ q\neq n}}^{\infty} \underline{\underline{\mathbf{G}}}(\mathbf{r}_{j,n},\mathbf{r}_{p,q}) \cdot \mathbf{p}_{p,q}, \qquad (1)$$

where $\underline{\underline{\mathbf{G}}}(\mathbf{r}_{j,n},\mathbf{r}_{p,q})$ is the electric-dipole dyadic GF [57,58]. By solving Eq. (1) in the absence of excitation ($\mathbf{E}^{\rm ext}_{j,n} = 0$), we can compute the guided/leaky wave eigenmodes supported by the chain. In this paper, we are only interested in the guided (bound) modes. An alternative representation of the fields can be accomplished via a combination of both spectral and spatial GFs, such as in the Ewald method for linear arrays [59–62].

Here, we make the following assumptions: (i) We consider a transverse polarization for which the excited dipole moments can be only oriented along the x direction, so that $\mathbf{p}_{j,n} = p_{j,n}\hat{\mathbf{x}}$; (ii) we only consider interactions within nearest neighbors scatterers, justified by the fact that interparticle distance is subwavelength. This approach, which resembles the TB formalism in solid-state physics [52,53,63], was also utilized in Refs. [48,50,64,65] to analyze the general properties of discrete interactions in $\mathcal{PT}$-symmetric systems. Following these assumptions, we can recast Eq. (1) in a much simpler form

$$\begin{aligned} p_{1,n} &= \alpha_1[G(d)p_{1,n+1} + G(d)p_{1,n-1}] + \\ &\quad + \alpha_2[G(b)p_{2,n+1} + G(a)p_{2,n} + G(b)p_{2,n-1}] \\ p_{2,n} &= \alpha_2[G(d)p_{2,n+1} + G(d)p_{2,n-1}] + \\ &\quad + \alpha_1[G(b)p_{1,n+1} + G(a)p_{1,n} + G(b)p_{1,n-1}], \end{aligned} \qquad (2)$$

where we have used the electric-dipole scalar GF $G(r) = G(\mathbf{r},\mathbf{r}') = k^3 \exp(ikr)[(kr)^{-3} - i(kr)^{-2} - (kr)^{-1}]/C$ [58,66], with $C = -4\pi\varepsilon_0\varepsilon_h$ (and ε_h being the dielectric constant of the host medium), $r = |\mathbf{r} - \mathbf{r}'|$ and $b = \sqrt{a^2 + d^2}$ (see Fig. 1), and k is the wave number in the host material. The equations in Eq. (2) can be cast in a form involving finite differences and a system evolution equation. However, our approach in this paper relies on the construction of a transfer matrix that relates the dipole moments at two locations $\mathbf{r}_{j,n}$ and $\mathbf{r}_{j,n+1}$, from which we can calculate the band structure of the periodic chain. To this aim, it is expedient to define a four-dimensional (4D) state vector as $\mathbf{\Psi}(n) = [p_{1,n}\ p_{2,n}\ p_{1,n-1}\ p_{2,n-1}]^T$ (with the superscript T denoting the transpose) which describes the spatial evolution of the dipole moments in the coupled chains. It is important to stress that, even though the choice of the state vector is not unique [67], the eigenvalues of the system are invariant under any nonsingular unitary (similarity) transformation of the state vector.

A. State vector evolution and transfer matrix

Using Eq. (2), we construct a discrete matrix equation for the state vector evolution as

$$\Psi(n+1) = \underline{\mathbf{T}}\,\Psi(n), \qquad (3)$$

where $\underline{\mathbf{T}}$ denotes the transfer matrix of the chain under the nearest neighborhood (i.e., TB) approximation. Such a matrix can be written as

$$\underline{\mathbf{T}} = \underline{\mathbf{M}}\,\underline{\mathbf{V}}, \quad \underline{\mathbf{M}} = \begin{pmatrix} -\underline{\underline{\mathbf{1}}} & \underline{\underline{\mathbf{A}}} \\ \underline{\underline{\mathbf{0}}} & -\underline{\underline{\mathbf{1}}} \end{pmatrix}, \quad \underline{\mathbf{V}} = \begin{pmatrix} \underline{\underline{\mathbf{0}}} & \underline{\underline{\mathbf{1}}} \\ -\underline{\underline{\mathbf{1}}} & \underline{\underline{\mathbf{0}}} \end{pmatrix}, \qquad (4)$$

where $\underline{\underline{\mathbf{1}}}$ is a 2×2 identity matrix, and $\underline{\underline{\mathbf{A}}}$ is a 2×2 matrix given by

$$\underline{\underline{\mathbf{A}}} = \begin{pmatrix} \frac{\alpha_2 G(d) + \alpha_1\alpha_2 G(a)G(b)}{\alpha_1\alpha_2\left(G^2(d) - G^2(b)\right)} & \frac{-\alpha_2 G(b) - \alpha_2^2 G(a)G(d)}{\alpha_1\alpha_2\left(G^2(d) - G^2(b)\right)} \\ \frac{-\alpha_1 G(b) - \alpha_1^2 G(a)G(d)}{\alpha_1\alpha_2\left(G^2(d) - G^2(b)\right)} & \frac{\alpha_1 G(d) + \alpha_1\alpha_2 G(a)G(b)}{\alpha_1\alpha_2\left(G^2(d) - G^2(b)\right)} \end{pmatrix}. \qquad (5)$$

The transfer matrix $\underline{\mathbf{T}}$, as in the context of layered media analysis [8,68], obeys some fundamental properties, such as $\det(\underline{\mathbf{T}}) = 1$ [9,69,70]; other spectral properties will be further discussed hereafter. We seek Bloch-type wave (periodic) solutions of Eq. (3) in the form

$$\mathbf{\Psi}(n+1) = \zeta\,\Psi(n), \qquad \zeta \equiv e^{ik_z d}, \qquad (6)$$

where k_z is a generally complex-valued Bloch wave number of the guided mode supported by the chain, with the sign of the real and imaginary part determining the forward/backward, and propagating/evanescent character, respectively, in a lossless structure. In the presence of gain and/or loss, these sign specifications may be violated in general. Note that a purely real-valued k_z means that power is conserved for that mode [64], and this may occur in chains with balanced gain and loss, as we show hereafter (see Sec. IV below). We emphasize that $e^{ik_z d}$ is the eigenvalue of Eq. (6), not the Bloch wave number k_z; however, it is natural to investigate the characteristics of k_z since it allows for a straightforward assessment of the gain and loss balance [71]. Bloch eigenmodes that satisfy Eqs. (3)

and (6) are derived from the eigenvalue problem

$$\underline{\mathbf{T}}\ \Psi_l(n) = \zeta_l\ \Psi_l(n), \tag{7}$$

where $\Psi_l(n)$ is the lth state eigenvector, with $l = 1,2,3,4$. This yields four eigenvalues and corresponding eigenvectors. Note that the homogenous solutions of Eq. (3) are constructed from the four eigenvectors in Eq. (7) in the case where the matrix $\underline{\mathbf{T}}$ can be diagonalized. When $\underline{\mathbf{T}}$ is not diagonalizable, i.e., at an EPD, generalized eigenvectorrs are used instead of the regular eigenvectors in Eq. (7) [22]. The four eigenvalues of Eq. (7) are determined from

$$\det[2\cos(k_z d)\underline{\underline{\mathbf{1}}} - \underline{\underline{\mathbf{A}}}] = 0, \tag{8}$$

which is further simplified to the transcendental form

$$4\cos^2(k_z d) - 2\cos(k_z d)\mathrm{Tr}(\underline{\underline{\mathbf{A}}}) + \det(\underline{\underline{\mathbf{A}}}) = 0. \tag{9}$$

Note that, from Eq. (9), we infer the symmetry property that both k_z and $-k_z$ are solutions, as expected in view of the time-inversion symmetry that is still valid under the small-signal and linear-gain assumptions. Depending on whether an EDP occurs or not, the number of independent eigenvectors that satisfy Eq. (7) may vary from one to four. Indeed, though not always possible in general, the transfer matrix $\underline{\mathbf{T}}$ may be diagonalized so that,

$$\underline{\mathbf{T}} = \underline{\mathbf{U}}\,\underline{\mathbf{\Lambda}}\,\underline{\mathbf{U}}^{-1}, \tag{10}$$

where $\underline{\mathbf{\Lambda}}$ is a diagonal matrix whose entries are the eigenvalues of Eq. (6), and $\underline{\mathbf{U}}$ implements a similarity transformation. In this case, there would be four independent system state eigenvectors.

B. EPDs

We now investigate a particular aspect of the dispersion diagram, namely, the emergence of EPDs. At an EPD, the matrix $\underline{\mathbf{U}}$ is singular, i.e., $\det[\underline{\mathbf{U}}] = 0$. Owing to the reciprocity ($\mathcal{T}$-inversion symmetry) restriction of the system, we can only attain two different kinds of degeneracies: (i) a second-order degeneracy at which two eigenstates coalesce, with a multiplicity $m = 2$ of the eigenstates; and (ii) a fourth-order degeneracy at which all eigenstates coalesce, with $m = 4$.

Accordingly, we investigate these two conditions in which the transfer matrix becomes similar to a matrix having Jordan blocks [72]. Under these conditions, a reduced number of regular eigenvectors will be found. In particular, when a fourth-order EPD occurs, Eq. (7) will possess one eigenvalue with multiplicity of four and only one regular eigenvector.

(i) *Second order EPD*. At a second-order EPD, the transfer matrix is written as

$$\underline{\mathbf{T}} = \underline{\mathbf{W}}\begin{bmatrix}\underline{\underline{\mathbf{\Lambda}}}^{+} & 0\\ 0 & \underline{\underline{\mathbf{\Lambda}}}^{-}\end{bmatrix}\underline{\mathbf{W}}^{-1},$$

$$\underline{\underline{\mathbf{\Lambda}}}^{+} = \begin{pmatrix}\zeta_e & 1\\ 0 & \zeta_e\end{pmatrix}, \quad \underline{\underline{\mathbf{\Lambda}}}^{-} = \begin{pmatrix}1/\zeta_e & 1\\ 0 & 1/\zeta_e\end{pmatrix}, \tag{11}$$

where $\zeta_e = e^{ik_e d}$ is the EPD eigenvalue of Eq. (7). The second-order EPD condition is found at an angular frequency $\omega = \omega_e$, and such degeneracy in the fundamental Brillouin zone $k_z \in [0,2\pi/d]$ occurs between two Bloch modes having $k_z \in [0,\pi/d]$ (denoted by the superscript $+$); the other two modes with $k_z \in [\pi/d,2\pi/d]$ (denoted by the superscript $-$) must also coalesce in view of the symmetry conditions of the eigenvalues solutions in Eq. (7). Here, $\underline{\underline{\mathbf{\Lambda}}}^{+}$ is a 2×2 Jordan block matrix and $\underline{\mathbf{W}}$ is constructed from two regular and two generalized basis eigenvectors. At $\omega = \omega_e$, homogenous solutions for the state vector in Eq. (3) are given in terms of two periodic (Bloch) modes having regular eigenvectors propagating as $e^{\pm ik_e nd}$ and two diverging solutions constructed from generalized eigenvectors that linearly grow as $nde^{\pm ik_e nd}$. It is important to point out that, near the second-order EPD, the wave number k_z can be written as a small perturbation of the ideal degeneracy condition with $k_z = k_e$, in terms of a fractional power expansion as

$$k_{z,l}(\omega) \cong (-1)^l k_e + h_l\delta^{1/2} + g_l\delta + \cdots, \tag{12}$$

where h_l and g_l are the fractional series expansion coefficients for the four modes with $l = \{1,2,3,4\}$, δ is a small perturbation parameter about the EPD, and the principal root of δ is taken. Such a perturbation parameter identifies the detuning from the ideal EPD condition in the spectral evolution of the states, which could be observed via frequency detuning, gain and loss imbalance, or asymmetry in the chain (or in any other structural parameter). We recall that the perturbation analysis of degenerate or defective operators requires one to deal with fractional power expansion, contrary to systems having only eigenvalue degeneracies (i.e., only coincident eigenvalues, but still a complete basis of eigenvectors [2,4,70,73]). As such, the fractional power series in Eq. (12), also known as Puiseux series, is a direct consequence of the Jordan block similarity [1,12,73]. In Sec. IV, we show the effect of two perturbation parameters (frequency detuning and gain-loss imbalance or asymmetry in the chain) separately and their consequences on $\mathcal{PT}$ symmetry and the second-order EPD.

(ii) *Fourth-order EPD*. At a fourth-order EPD, the transfer matrix becomes similar to a 4D Jordan matrix

$$\underline{\mathbf{T}} = \underline{\mathbf{S}}\underline{\mathbf{\Lambda}}\,\underline{\mathbf{S}}^{-1}, \quad \underline{\mathbf{\Lambda}} = \begin{pmatrix}\zeta_e & 1 & 0 & 0\\ 0 & \zeta_e & 1 & 0\\ 0 & 0 & \zeta_e & 1\\ 0 & 0 & 0 & \zeta_e\end{pmatrix}, \tag{13}$$

thereby implying a fourth-order degeneracy between all Bloch modes in the 4×4 system. Here, $\underline{\mathbf{\Lambda}}$ is a 4×4 Jordan matrix, and $\underline{\mathbf{S}}$ is constructed from one regular and three generalized basis eigenvectors. In this particular case, we find that $\zeta_e = -1$. At $\omega = \omega_e$, homogenous solutions for the state vector in Eq. (3) at the fourth-order EPD are given in terms of one Bloch periodic mode having a regular eigenvector in Eq. (7) that propagates as $e^{ik_e nd}$, and three non-Bloch (nonperiodic) diverging solutions constructed from a generalized set of eigenvectors growing as $nde^{ik_e nd}$, $(nd)^2 e^{ik_e nd}$, and $(nd)^3 e^{ik_e nd}$ [22,70]. Similar to the second-order EPD, the wave number near a fourth-order EPD asymptotically follows the fractional power expansion

$$k_{z,l}(\omega) \cong k_e + h_l\delta^{1/4} + g_l\delta^{2/4} + \cdots, \tag{14}$$

where h_l and g_l are the fractional series expansion coefficients for the nth eigenmodes, and δ is the perturbation factor.

In what follows, we quantitatively investigate the modal dispersion characteristics near a second- and fourth-order EPD

of a chain composed of a pair of dipolar scatterers with gain and loss.

IV. EPD AND $\mathcal{PT}$ SYMMETRY IN GAIN- AND LOSS-BALANCED COUPLED CHAIN

As mentioned in the previous section, degenerate states, if they exist, are characterized not only by the multiplicity of the eigenvalues in Eq. (7) but also by their geometric multiplicity, i.e., the linear dependence of the eigenvectors [1,3,6,72,74]. We assume that the wave number of the degenerate state is denoted by $\pm k_e$. Therefore, by invoking the eigenvalue multiplicity and symmetry conditions, the dispersion relation in Eq. (9) at the EPD takes the form

$$[\cos(k_z d) - \cos(k_e d)]^2 = 0. \tag{15}$$

Moreover, when an EPD occurs, the transfer matrix $\underline{\underline{\mathbf{T}}}$ in Eq. (4) can only be written in terms of Jordan blocks and not in terms of diagonalized matrices. To derive the conditions on the polarizabilities of the coupled chain's scatterers in order for an EPD to occur, we compare Eq. (9) with Eq. (15) and obtain two conditions on the characteristic matrix $\underline{\underline{\mathbf{A}}}$, viz.

$$\mathrm{Tr}(\underline{\underline{\mathbf{A}}}) = 4\cos(k_e d), \quad \text{and} \quad \det(\underline{\underline{\mathbf{A}}}) = 4\cos^2(k_e d). \tag{16}$$

Equation (16), along with Eq. (13), imposes the following conditions:

$$\begin{aligned} \alpha_1^e \alpha_2^e &= \frac{1}{4\cos^2(k_e d)(G^2(d) - G^2(b)) + G^2(a)} \equiv \xi, \\ \left(\alpha_1^e + \alpha_2^e\right) &= \frac{-2G(a)G(b) + 4(G^2(d) - G^2(b))\cos(k_e d)}{[4\cos^2(k_e d)(G^2(d) - G^2(b)) + G^2(a)]G(d)} \\ &\equiv \chi, \end{aligned} \tag{17}$$

where $\alpha_1^e \equiv \alpha_1(\omega_e)$ and $\alpha_2^e \equiv \alpha_2(\omega_e)$ are the required values for the polarizability to achieve a second- or fourth-order EPD at a wave number k_e and angular frequency ω_e. Another necessary condition, besides Eq. (17), is that $\det[\underline{\mathbf{U}}] = 0$, which is implicitly satisfied from Eq. (16) through the constraint $\mathrm{Tr}^2(\underline{\underline{\mathbf{A}}}) = 4\det(\underline{\underline{\mathbf{A}}})$. Accordingly, the conditions in Eq. (17) on the polarizabilities are necessary and sufficient to attain the required EPD. The polarizabilities are obtained as solutions of Eq. (17) in terms of $\xi = \alpha_1^e \alpha_2^e$ and $\chi = \alpha_1^e + \alpha_2^e$ as

$$\alpha_{1,2}^e = \frac{\chi \pm \sqrt{\chi^2 - 4\xi}}{2}, \tag{18}$$

for an EPD occurring at an angular frequency ω_e. We highlight that some trivial conditions exist for the chain to develop an EPD, such as at zero frequency. In what follows, we focus on nontrivial EPDs, namely second- and fourth-order, in the presence of both gain and loss. We refer to gain and loss balance as the general condition that guarantees the existence of an EPD in the spectrum of a coupled system described by non-Hermitian evolution equations as discussed in Ref. [72]. Indeed, $\mathcal{PT}$ symmetry is not a necessary condition for developing an EPD, as shown in Refs. [72,75]. The more general balance condition is revealed in the chains when Eq. (18) is satisfied, resulting in an EPD in the dispersion diagram. Within this framework, $\mathcal{PT}$ symmetry is a special case, which would also lead to observing an EPD as discussed in the following. It is worth mentioning that completely lossy chains (e.g., with asymmetric distributions of loss in the polarizabilities) can also exhibit effects related to EPDs. These effects, typically referred to as passive $\mathcal{PT}$ symmetry [39], could lead to loss-induced transmission and other interesting phenomena. However, here, we only focus on EPDs associated with gain and loss balance.

A. Second-order EPD and $\mathcal{PT}$ symmetry

A second-order degeneracy indicates that the solutions $\zeta_{e,l}$ of the system in Eq. (7) can take the values $\zeta_{e,1} \equiv \zeta_e \equiv e^{ik_e d}$ and $\zeta_{e,2} \equiv 1/\zeta_e \equiv e^{-ik_e d}$, with $k_e d \neq \pi$, i.e., away from the center of the Brillouin zone (defined here as the interval $k_z \in [0, 2\pi/d]$). Indeed, $k_z = \pi/d$ is the center of Brillouin zone where modes naturally coalesce, and it is well known to be a point where the group velocity vanishes if a bandgap exists [8,70]. To gain some physical insight into the conditions above, it is important to explore how the polarizabilities of the chain are constrained for an EPD to occur. We investigate different regimes of operations based on quasistatic approximations and the effect of phase retardation on the EPD conditions.

(i) *Quasistatic limit.* This applies when $kr \to 0$, with r being an arbitrary observation distance. Consequently, the GF follows its electrostatic limit $G(r) \to 1/(C\, r^3)$. It is straightforward to see that, under such a condition, an EPD can occur provided that $(\alpha_1^e + \alpha_2^e)^2 < 4\alpha_1^e \alpha_2^e$, since $G(d) > G(b)$ (the GF is real under this limiting case). Therefore, by enforcing the conditions for an EPD to occur [Eqs. (17) and (18)], we obtain the conjugate symmetry condition

$$\alpha_1^e = \left(\alpha_2^e\right)^*. \tag{19}$$

This condition implies that, when such low-frequency EPD occurs, one chain exhibits losses, and the other exhibits gain that precisely compensates for the losses. This condition is inherently tied with the aforementioned $\mathcal{PT}$ symmetry concept. As typical in $\mathcal{PT}$-symmetric systems, the EPD is related to the spontaneous symmetry breaking phenomenon, and it constitutes the boundary that separates the exact and broken phases characterized by real- and complex-valued eigenspectra, respectively. Such a condition was rigorously satisfied in uniform coupled wave guides [29,30,72,76], and here, we showed that it holds in connection with periodic coupled chains of scatterers as well. Effects of field-retardation corrections in the GF are discussed next.

(ii) *Effect of GF phase retardation.* The $\mathcal{PT}$ symmetry with perfectly symmetric gain and loss balance governed by Eq. (19) is relevant when $kr \to 0$ corresponding to the quasistatic case described in the previous subsection. However, when phase propagation is included in the GF, i.e., kr assumes finite values, radiation losses exist due a nonvanishing imaginary part of the GF [57]. It is important to point out that both radiation losses and absorption mechanisms contribute to the scatterers' polarizabilities. Accordingly, even when the scatterers have intrinsic gain, radiation losses would notably affect the imaginary part of their polarizability α in the short-wavelength limit. However, thanks to the deeply subwavelength interparticle distances (long wavelengths) considered here and the strong near-field interaction, the quasistatic interpretation of the polarizabilities as well as the classification of gain and loss described in Sec. II still hold. Therefore, at

TABLE I. Required chain polarizabilities to realize a second-order EPD at different normalized frequencies.

$\omega_e d/c$	$\alpha_1^e \times 10^{32}$ [$C\,\mathrm{m}^2\mathrm{V}^{-2}$]	$\alpha_2^e \times 10^{32}$ [$C\,\mathrm{m}^2\mathrm{V}^{-2}$]
0.02	$-3.59 - i4.97$	$-3.59 + i4.97$
0.1	$-3.61 - i4.99$	$-3.61 + i4.98$
0.5	$-3.93 - i6.06$	$-4.18 + i4.74$

an EPD, one expects that the conjugate-symmetry condition in Eq. (19) is no longer rigorously satisfied due to the extra radiation (scattering) losses in the chain. Nevertheless, as we show below, an EPD can still occur since a gain-loss balance can be achieved from the condition in Eq. (18). On the other hand, if one chooses the perfect conjugate symmetry condition in Eq. (19) on the chain, an ideal EPD (where the eigenvectors are rigorously degenerate) can no longer be identified. Furthermore, such additional radiation losses (at high frequencies) could be manipulated and engineered to produce effects related to EPDs, such as loss-induced transmission [39]. Here, the analysis of lossy chains of infinite length is omitted because it would require the use of an infinitely periodic GF [59–62], whereas our main scope is to provide a simple but intuitive analysis based on the nearest-neighbor approximation, that resembles the TB approach used in Refs. [48,50,64,65].

We consider an example of a chain in vacuum (i.e., $\varepsilon_h = 1$) with $a = d = 100$ nm, and we select the EPD wave number to be $k_e d = \pi/5$, with $\omega_e d/c = 0.02$. This frequency implies that the period $d \approx 0.003\lambda_e$ (where $\lambda_e = 2\pi c/\omega_e$ is the wavelength in vacuum) is deeply subwavelength, thereby justifying the low-frequency assumption. By assuming the polarizabilities as frequency independent in the vicinity of ω_e, we obtain the values $\alpha_1 \cong \alpha_2^* = (-3.59 - i4.97) \times 10^{-32}$ [$C\,\mathrm{m}^2\mathrm{V}^{-2}$] (see Table I), in order to attain a second-order EPD at $\omega_e d/c = 0.02$. These values approximately satisfy Eq. (19) because of the low-frequency choice for this EPD to occur. In Fig. 3, we show the dispersion relationship of the two modes exhibiting the EPD. We only show the positive real part of the complex wave number within the region $\mathrm{Re}(k_z) \in [0,\pi/d]$, but we stress that the wave number branches satisfying $\mathrm{Re}(k_z) \in [\pi/d,2\pi/d]$ also exhibit the EPD thanks to reciprocity. In Fig. 4, we also show the determinant (magnitude) of the similarity matrix $\mathbf{U}$, which represents a quantitative metric of the closeness to an EPD condition. Indeed, at $\omega = \omega_e$, we observe that $|\det(\underline{\mathbf{U}})| \to 0$, indicating that the system eigenvectors coalesce and cease to form a complete basis set [1,2,30]. As previously explained, exactly at the EPD, there is no similarity transformation that diagonalizes the transfer matrix $\underline{\mathbf{T}}$, which in turn becomes similar to a matrix with Jordan blocks as in Eq. (11). In Fig. 5, we show the mode evolution in the complex k_z plane [$\mathrm{Re}(k_z) - \mathrm{Im}(k_z)$ plane] as the frequency increases. As it can be observed, the modal wave numbers are almost real, i.e., $|\mathrm{Im}(k_z)/\mathrm{Re}(k_z)| < 10^{-3}$ for $\omega < \omega_e$, and become almost complex conjugate pairs for $\omega > \omega_e$. Modes with purely real k_z for $\omega < \omega_e$ are a fundamental consequence of the perfect gain-loss balance and symmetry of the system obeying an exact phase of $\mathcal{PT}$ symmetry, for long wavelength. Conversely, for $\omega > \omega_e$, such properties are violated, even though the gain and loss conjugate symmetry in Eq. (19) is satisfied, and

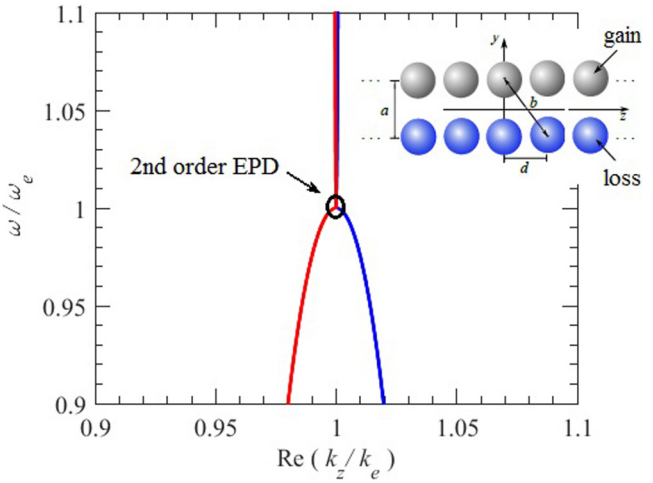

FIG. 3. Dispersion diagram of the two modes with positive $\mathrm{Re}(k_z)$ exhibiting an EPD at ω_e. The $\mathcal{PT}$ symmetry allows for real modes when the gain-loss balance and symmetry condition in Eq. (19) is satisfied below the EPD ($\omega < \omega_e$). Here, $d = a = 100$ nm, $\omega_e d/c = 0.02$ and $k_e = \pi/(5d)$, and the polarizabilities of the chain are given in Table I.

the system enters the broken phase. By setting $\delta \equiv (\omega - \omega_e)$ in Eq. (12), and limiting the fractional power series to the first-order term, the asymptotic dispersion relationship near such a second-order EPD is given by $[k_{z,l} - (-1)^l k_e]^2 \cong h_l^2 \delta$, where $h_l^2 = 2\partial^2 k_{z,l}/\partial\omega^2$ at $\omega = \omega_e$.

We also investigate the detuning of the second-order EPD by varying the gain and loss values implemented in the polarizabilities from their optimal condition Eq. (18). For that purpose, we assume an exact gain and loss symmetry in the chain, i.e., $\alpha_{1,2} = \alpha'(1 \pm i\gamma)$, with the gain and loss normalized factor γ defined as $\gamma = |\alpha''/\alpha'|$. We are interested in exploring how the mode characteristics change by varying the gain and loss factor γ. In Fig. 6, we show the positive branches of k_z for two different normalized EPD frequencies $\omega_e d/c$, varying as a function of γ for a chain with parameters $d = a = 100$ nm, and we choose $\alpha' = \mathrm{Re}(\alpha_1^e)$ from Table I for each value of $\omega_e d/c$. We clearly observe the occurrence of the EPD for the smaller electrical period ($\omega_e d/c = 0.02$). Moreover, the exact $\mathcal{PT}$-symmetric phase is observed at that frequency for a gain-loss parameter γ less than a critical value

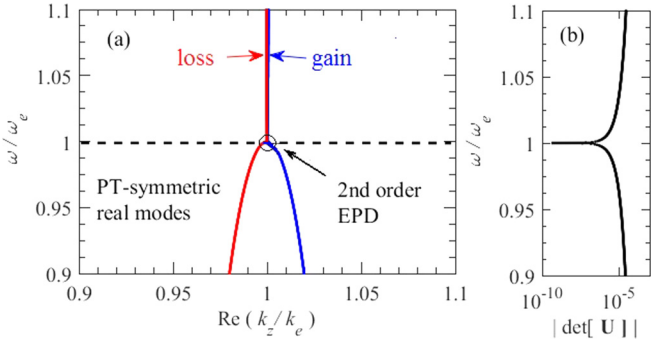

FIG. 4. (a) Same as Fig. 3. (b) Magnitude of the determinant of matrix $\underline{\mathbf{U}}$ that brings the transfer matrix into a diagonal form in Eq. (10).

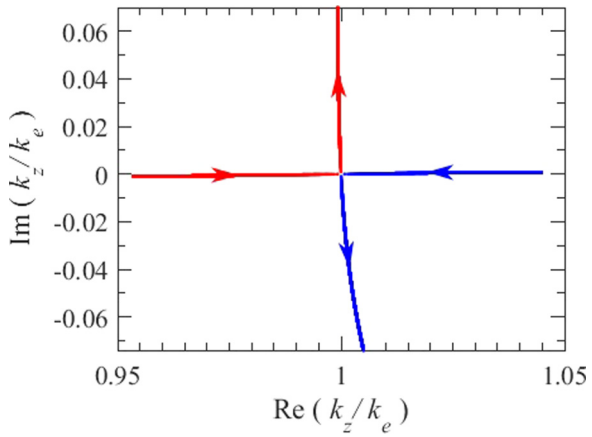

FIG. 5. Complex modal k_z trajectory in the[Re(k_z)-Im(k_z)] plane varying as a function of frequency showing the modes coalescing at the second-order EPD at $k_z = k_e$. Arrows show increasing frequency. Here, we used the same chain's parameters as in Fig. 3.

($\gamma \simeq 1.35$). At $\gamma \simeq 1.35$, the system undergoes spontaneous $\mathcal{PT}$ symmetry breaking, designating the EPD, and beyond this threshold, the modes cease to be real. However, for the higher-frequency case $\omega_e d/c = 0.1$, the EPD can no longer be attained with the exact gain and loss symmetry. Instead, as discussed previously, an asymmetry must be introduced due to radiation losses. In this connection, the reader is also referred to Ref. [72] in which different figure of merits were proposed in order to assess the quality or evidence of such an EPD subject to perturbation due to disorders and imperfect gain and loss balance. To further elucidate this aspect, we also show the dispersion relationships of the modes belonging to a chain in which the polarizabilities are obtained from the symmetry design Eq. (19) to exhibit a second-order EPD. We consider two frequencies for which $\omega_e d/c = 0.1$ and $\omega_e d/c = 0.5$ (i.e., increasing the frequency or period with respect to the case shown in Fig. 4) in Figs. 7 and 8, respectively. The

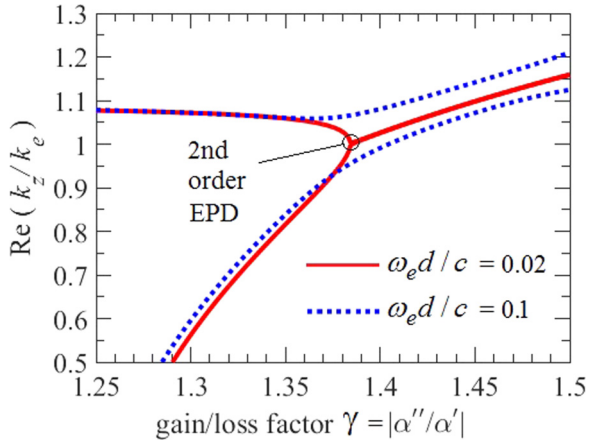

FIG. 6. Positive branch of Re[k_z] varying as a function of the gain-loss parameter $\gamma = |\alpha''/\alpha'|$, demonstrating the detuning near a second-order EPD for two cases of the normalized frequency $\omega_e d/c$. Chain parameters are as in Fig. 3. Note that the perfect gain-loss symmetry condition does not provide a clear EPD for the case with higher frequency.

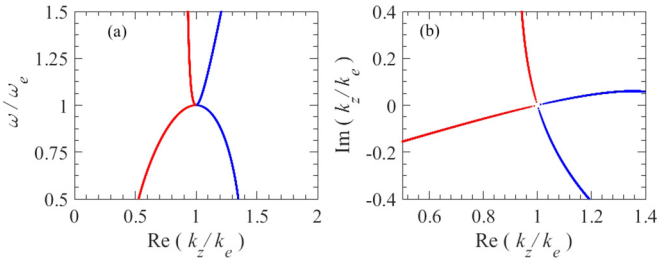

FIG. 7. (a) Dispersion diagram [Re(k_z)-ω] and (b) complex k_z trajectory varying as a function of frequency of a chain, developing a second-order EPD at $\omega_e d/c = 0.1$. Here, we used the same chain's parameters as in Fig. 3, except that the EPD is designed to occur at higher frequency.

corresponding polarizabilities of the chain that are evaluated from Eq. (18) to realize the EPD conditions at the above mentioned frequencies are $\alpha_1 = (-3.61 - i4.99) \times 10^{-32}$ [$C\,m^2V^{-2}$], $\alpha_2 = (-3.61 + 4.98) \times 10^{-32}$ [$C\,m^2V^{-2}$] for $\omega_e d/c = 0.1$, and $\alpha_1 = (-3.94 - i6.06) \times 10^{-32}$ [$C\,m^2V^{-2}$], $\alpha_2 = (-4.19 - i4.74) \times 10^{-32}$ [$C\,m^2V^{-2}$] for $\omega_e d/c = 0.5$ (see Table I). We highlight that, when the frequency increases, the required polarizabilities α_1 and α_2 to attain an EPD do not satisfy the perfect conjugate symmetry condition in Eq. (19). In addition, it can be observed from the complex k_z trajectories in Figs. 7(b) and 8(b) that the modes no longer have purely real k_z values for $\omega < \omega_e$, especially for larger $\omega_e d/c$. Nonetheless, the EPD occurrence at ω_e is evident, even when gain and loss are not symmetric. We point out that, near the EPD in Figs. 7 and 8, in view of the frequency detuning, modes tend to lose symmetry around $k_z = k_e$, meaning that the gain and loss asymmetry causes another form of perturbation near the EPD, especially at high frequencies. In order to capture this asymmetry, one should consider additional terms in the fractional power series expansion Eq. (12).

B. Fourth-order EPD and DBE

A fourth-order degeneracy indicates that all four eigenstates of the system in Eq. (7) coalesce, and this can only be in the form $\zeta_e \equiv e^{ik_e d}$ with $\zeta_e = -1$, i.e., $k_e d = \pi$. This condition occurs in the middle of the band edge of the periodic structure's Brillouin zone $k_z \in [0, 2\pi/d]$. For lossless structures, this condition has been conventionally referred to

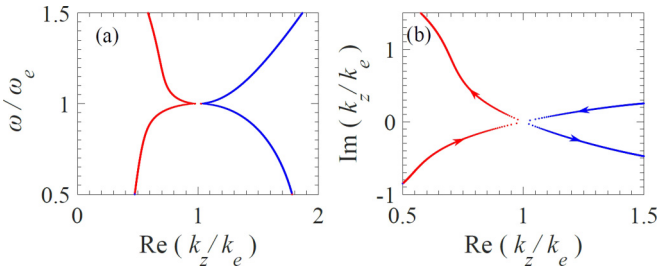

FIG. 8. (a) Dispersion diagram [Re(k_z)-ω] and (b) complex k_z trajectory varying as a function of frequency of a chain, developing a second-order EPD at $\omega_e d/c = 0.5$. Here, we used the same chain's parameters as in Fig. 3, but the EPD frequency is even higher than that in Fig. 7.

TABLE II. Required chain polarizabilities to realize a fourth-order EPD at different normalized frequencies.

$\omega_e d/c$	$\alpha_1^e \times 10^{32}$ [$C\,\mathrm{m}^2\mathrm{V}^{-2}$]	$\alpha_2^e \times 10^{32}$ [$C\,\mathrm{m}^2\mathrm{V}^{-2}$]
0.02	$5.2 - i0.68$	$5.2 + i0.68$
0.1	$5.22 - i0.69$	$5.22 + i0.68$
0.5	$6.05 - i0.45$	$5.37 + i1.19$

as DBE. Typical examples of DBE effects have been shown in lossless photonic crystals as in Refs. [12,13,16,17] and other wave guiding structures [24,25]. Here, however, we show that the chain develops this fourth-order EPD thanks to the gain-loss interplay and taking advantage of the natural mode coalescence at the band edge. For the same parameters of the chain discussed in Sec. IV A, we select $\omega_e d/c = 0.02$ and $k_e d = \pi$. Under this condition, an EPD is attained for $\alpha_1^e \cong (\alpha_2^e)^* = (5.2 - i0.68) \times 10^{-32}$ [$C\,\mathrm{m}^2\mathrm{V}^{-2}$] (see Table II for α_1^e and α_2^e). The corresponding dispersion relation is shown in Fig. 9(a). Once again, also shown [in Fig. 9(b)] is $|\det(\underline{\mathbf{U}})|$, which vanishes at ω_e. Similar to the second-order EPD example in Fig. 4, the period is deeply subwavelength ($d \approx 0.003\lambda_e$) and the EPD condition corresponds to the perfect gain and loss balance and conjugate symmetry condition in Eq. (19).

By letting $\delta \equiv (\omega - \omega_e)$ in Eq. (14), and retaining the first term, the asymptotic dispersion relation near such fourth-order degeneracy is given by $(k_z - k_e)^4 \cong h^4\delta$, with $h^4 = 24\,\partial^4 k_z/\partial\omega^4$ at $\omega = \omega_e$ and $k_z = k_e$. Figure 10 shows the complex k_z trajectory, as a function of frequency. We observe branches of purely real k_z modes and two branches of complex conjugates ones, for $\omega < \omega_e$, coalescing at the EPD for $\omega = \omega_e$, and then evolving into four complex modes for $\omega > \omega_e$.

We also illustrate in Fig. 11 the detuning from the fourth-order EPD by varying the gain and loss parameter γ defined in Sec. IV A, i.e., having conjugate symmetry in the polarizabilities, $\alpha_{1,2} = \alpha'(1 \pm i\gamma)$. More specifically, we show the positive branches of $\mathrm{Re}(k_z)$ for two different normalized frequencies $\omega_e d/c$, with the corresponding $\alpha' = \mathrm{Re}(\alpha_1^e)$ taken from Table II for each case.

Analogous to the second-order EPD, the occurrence of the fourth-order EPD with perfectly balanced gain-loss and

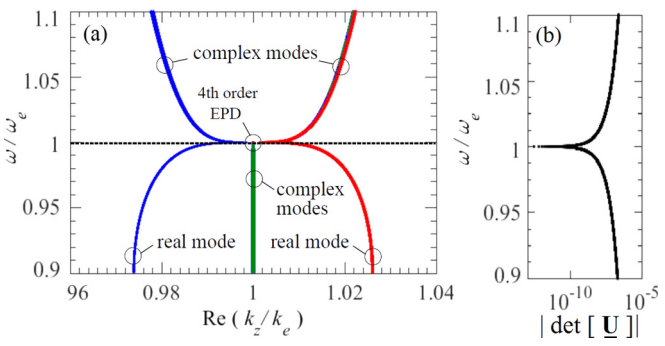

FIG. 9. (a) Dispersion diagram [$\mathrm{Re}(k_z)$-ω] of the four modes of the chain exhibiting a fourth-order degeneracy at the band edge, and (b) the corresponding magnitude of the determinant of similarity $\underline{\mathbf{U}}$. The chain has $d = a = 100$ nm with $\omega_e d/c = 0.02$ and $k_e = \pi/d$.

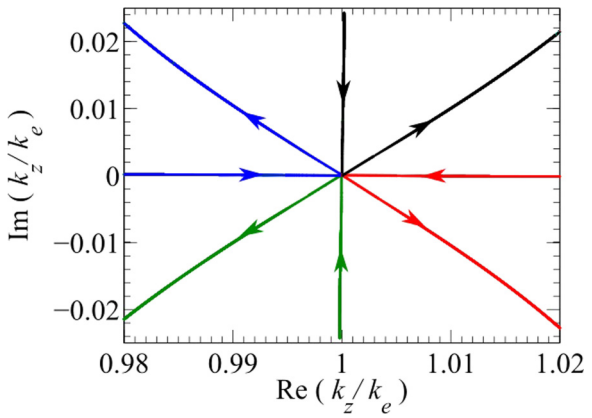

FIG. 10. Complex k_z trajectory plane varying as a function of frequency with the four modes coalescing at k_e. The chain has the same parameters used in Fig. 9.

complex-conjugate polarizabilities (i.e., $\mathcal{PT}$-symmetric) is evident for the smaller electrical period ($\omega_e d/c = 0.02$), but it does not hold for the case with $\omega_e d/c = 0.1$. Once again, large values of $\omega_e d/c$ imply that the dispersion relation is deformed in the vicinity of the gain-loss balance condition at which an EPD is expected ($\gamma \approx 0.132$), and the EPD is no longer observable (as seen in Fig. 11 for the case with $\omega_e d/c = 0.1$).

For better illustration, we show in Figs. 12 and 13 the dispersion relationships and the complex k_z trajectories near the fourth-order EPD for $\omega_e d/c = 0.1$ and $\omega_e d/c = 0.5$, respectively. Once again, the occurrence of a fourth-order EPD is possible, without requiring conjugate symmetry of the polarizabilities. The corresponding polarizabilities of the chain are $\alpha_1^e = (5.22 - i0.69) \times 10^{-32}$ [$C\,\mathrm{m}^2\mathrm{V}^{-2}$], $\alpha_2^e = (5.22 + i0.68) \times 10^{-32}$ [$C\,\mathrm{m}^2\mathrm{V}^{-2}$] for $\omega_e d/c = 0.1$, and $\alpha_1^e = (6.05 - i0.45) \times 10^{-32}$ [$C\mathrm{m}^2\,\mathrm{V}^{-2}$], $\alpha_2^e = (5.37 + i1.19) \times 10^{-32}$ [$C\mathrm{m}^2\,\mathrm{V}^{-2}$] for $\omega_e d/c = 0.5$ (see Table II). Results in Figs. 12 and 13 show that the wave

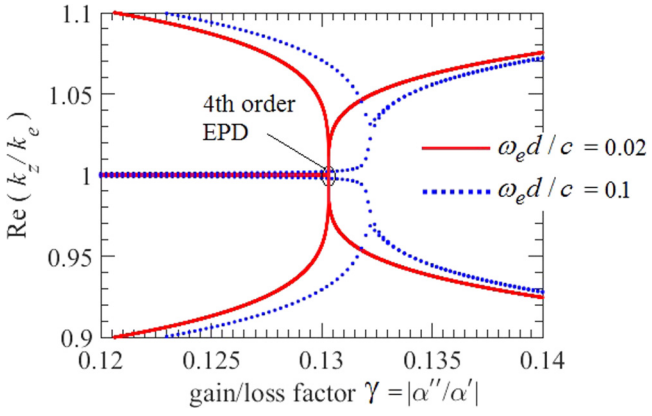

FIG. 11. Positive branch of $\mathrm{Re}[k_z]$ varying as a function of the gain-loss parameter $g = |\alpha''/\alpha'|$, demonstrating the detuning near a fourth-order EPD for two cases of the normalized frequency $\omega_e d/c$. Chain parameters are as in Fig. 9 and $\alpha' = \mathrm{Re}(\alpha_1^e)$ is taken from Table II for each case. Note that the perfect gain-loss symmetry condition does not provide a clear EPD for the case with higher frequency.

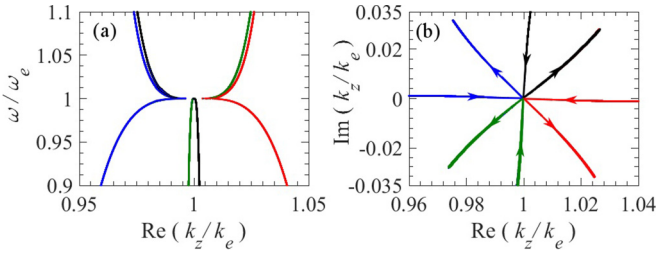

FIG. 12. (a) Dispersion diagram [Re(k_z)-ω] and (b) complex k_z trajectory varying as a function of frequency of a chain, developing a fourth-order EPD at $\omega_e d/c = 0.1$. The chain has the same parameters used in Fig. 9.

number trajectory around the fourth-order EPD frequency behaves differently compared to the case in Fig. 9, suggesting that one should consider a larger number of terms in Eq. (14) to approximate the eigenstate characteristics (eigenvalue and eigenvectors) near the EPD frequency. The same conclusion applies when other structural parameters are detuned. Nevertheless, by proper tuning of the polarizabilities, one can still attain the remarkable features of fourth-order EPDs, in terms of a high Q factor due to a dramatic reduction group velocity.

As a concluding remark, it is worth highlighting that the perturbation of the fourth-order EPD eigenstate with frequency or imbalance of gain and loss is much stronger than the second-order counterpart, since the perturbation factor δ in the fractional expansions in Eqs. (12) and (14) dictates that $|\delta|^{1/4} > |\delta|^{1/2} > |\delta|$ for $|\delta| \ll 1$. Accordingly, a small structural perturbation can lead to a significant measurable modification of the spectral evolution of the system near these EPDs, leading to strongly enhanced sensitivity. This can find important applications to sensing [74].

V. EPD IN A COUPLED CHAIN OF NANOSPHERES WITH FREQUENCY-DEPENDENT PARAMETERS

We now demonstrate a realistic example of EPDs occurring in a chain of spherical nanoparticles at optical frequencies, by considering metals and optically pumped active materials, and by also taking into account the frequency-dependent behavior of the nanoparticles polarizabilities. Referring to the geometry schematized in Fig. 14(a), we begin by assuming $a = d = 32$ nm. The passive nanosphere with polarizability α_2 is made

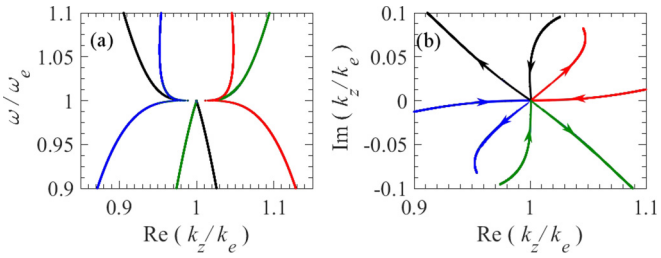

FIG. 13. (a) Dispersion diagram [Re(k_z) − ω] and (b) complex k_z trajectory varying as a function of frequency, for a chain with the same geometrical parameters used in Fig. 9. It develops a fourth-order EPD at $\omega_e d/c = 0.5$ when the perfect gain/loss symmetry condition does not hold anymore.

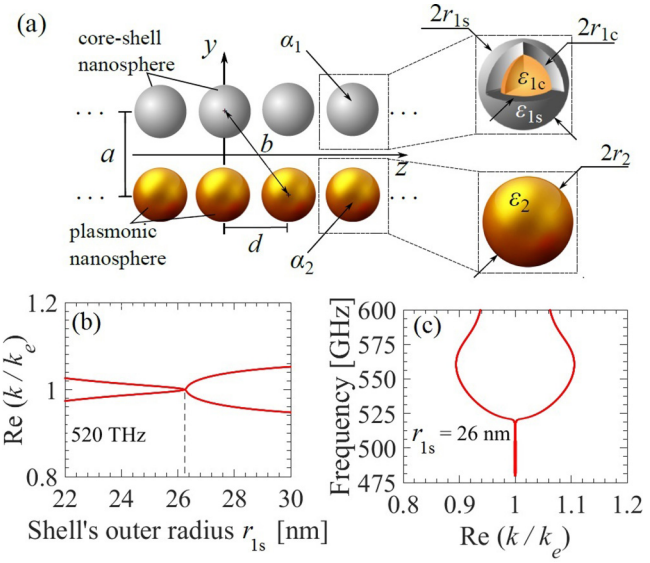

FIG. 14. (a) Example of a coupled chain with gain and loss balance made of pairs of plasmonic nanosphere and a core-shell nanosphere with active core. The chain exhibits an EPD at optical frequencies. (b) Two branches of Re[k_z] varying shell's radius at 520 THz, in which the chain exhibits a second-order EPD when $r_{1s} \approx 26$ nm. (c) Dispersion diagram [Re(k_z) − ω] of the two branches in (b) when $r_{1s} = 26$ nm that shows a second-order EPD at ~520 THz and $k_e = \pi/d$. Here, $a = d = 32$ nm, the gold nanosphere radius is $r_2 = 20$ nm, while and all other parameters are kept constant and reported in the Appendix.

of gold, while the active particle is realized by a core-shell nanosphere with a gold shell and a silica core doped with active fluorescent molecules (Rhodamine 6G dyes).

For the gold nanosphere and nanoshell, we consider the Drude-type dispersive model in the Appendix. A description of the steady-state linearized relative permittivity for the gain material can be found in several textbooks, such as Ref. [77], and more specifically in Ref. [56] for nanoshells (see also the Appendix). We assume that each of the gold nanospheres has a radius of 20 nm. The EPD is realized for a specific gain and loss balance condition. As illustrated in Fig. 14(b), this is attained by varying the shell's outer radius, namely r_{1s}, while keeping the core-to-shell radius ratio r_{1s}/r_{1c} fixed, as well as all the other parameters. We assume a frequency of 520 THz, which lies within the emission band of the core's fluorescent dyes [78] (see Appendix). Accordingly, we find the radius at which an EPD occurs by plotting k_z versus r_{1s}; we obtain $r_{1s} \approx 26$ nm. Figure 14(c) shows the corresponding dispersion diagram for $r_{1s} = 26$ nm, from which a second-order EPD is clearly visible at 520 THz. We emphasize that, for this parameter configuration, the chain does not satisfy the $\mathcal{PT}$ symmetry balance condition in Eq. (19), i.e., $\alpha_1 \neq \alpha_2^*$ at 520 THz (see the corresponding values in the Appendix). These findings verify the capability of realizing EPDs in simple yet realistic structures made of lossy/active nanospheres, without the need for sophisticated numerical optimization. Furthermore, this example can be generalized to more complex scatterers' geometries of nanorods on substrates, which can be further optimized for experimental demonstration.

VI. CONCLUSIONS AND DISCUSSION

We have demonstrated the occurrence of EPDs of second and fourth order in coupled linear chains of scatterers with properly tuned gain and loss in the dipolar polarizabilities. We also have elucidated possible connections with the $\mathcal{PT}$-symmetry concept. In addition, we have discussed the impact of gain and loss imbalance as well as conjugate asymmetry of the scatterers' polarizabilities on both second- and fourth-order EPDs. Our results rely on a TB-based approach formulated in terms of transfer matrix. Furthermore, we have demonstrated a realistic EPD implementation in a coupled chain made of plasmonic nanospheres and active core-shell nanospheres at optical frequencies. We highlight that the TB approach is an approximation of the more accurate fully periodic GF method [61,62]. Nonetheless, we have observed good agreement between the TB approach and the fully periodic GF in analyzing the scattering properties of finite chains with balanced gain and loss near a long-wavelength EPD, as typical in photonic bandgap structure analyses [52]. These aspects will be investigated more in depth in future studies.

Our analysis provides some insights into how EPDs can manifest in general discrete coupled mode structures. These properties can also be harnessed for sensing applications, enhancing nonlinear effects (including second harmonic generation and unprecedented soliton propagation), as well as lowering the threshold for lasing (as demonstrated in Ref. [16] for lossless DBE structures with extrinsic gain). Moreover, the structures of interest can be implemented by using plasmonic particles for applications ranging from near-field enhancement to super-resolution at optical wavelengths.

ACKNOWLEDGMENTS

This material is based upon work supported by the Air Force Office of Scientific Research under award number FA9550-15-1-0280 and under the Multidisciplinary University Research Initiative award number FA9550-12-1-0489 administered through the University of New Mexico.

APPENDIX: DETAILS PERTAINING TO SEC. V

The polarizability of a plasmonic spherical nanoparticle, assumed to be in vacuum, is given by the Clausius-Mossotti formula (see p. 8–6 in [79])

$$\alpha_2 = 4\pi r_2^3 \varepsilon_0 \left[\frac{\varepsilon_2 + 2}{\varepsilon_2 - 1} - i\frac{2(kr_2)^3}{3}\right]^{-1}, \tag{A1}$$

where r_2 is the radius of the nanosphere, and the imaginary term in the parentheses takes into account the radiation losses. Moreover, the relative permittivity ε_2 is provided by the Drude model as

$$\varepsilon_2 = \varepsilon_\infty - \frac{\omega_p^2}{\omega(\omega + i\Gamma)}, \tag{A2}$$

where ω_p is the plasma angular frequency, Γ is the damping factor, and ε_∞ is the high-frequency permittivity limit. The core-shell particle polarizability, including radiation losses, is given by [56]

$$\alpha_1 = \left[\frac{1}{4\pi\varepsilon_0 r_{1s}^3}\frac{(\varepsilon_{1s}+2)(\varepsilon_{1c}+2\varepsilon_{1s}) + 2\beta(\varepsilon_{1s}-1)(\varepsilon_{1c}-\varepsilon_{1s})}{(\varepsilon_{1s}-1)(\varepsilon_{1c}+2\varepsilon_{1s}) + \beta(2\varepsilon_{1s}+1)(\varepsilon_{1c}-\varepsilon_{1s})} - i\frac{k^3}{6\pi\varepsilon_0}\right]^{-1}, \tag{A3}$$

where ε_{1c} is the relative permittivity of the core (whose radius is r_{1c}), ε_{1s} is the relative permittivity of the shell (whose outer radius is r_{1s}) and $\beta = (r_{1c}/r_{1s})^3$. The shell is assumed to be made of gold, with relative permittivity ε_{1s} provided by the Drude model, i.e., $\varepsilon_{1s} = \varepsilon_2$. The active core has an effective relative permittivity ε_{1c} given by an inverted Lorentzian frequency line shape. The effective model of the gain material made of a concentration of fluorescent dye molecules is described by a four-level atomic system, and the formulation can be found in several textbooks [77,80] (see also Refs. [56,81]). Here, we limit ourselves to provide the effective linearized relative permittivity at steady state [56]

$$\varepsilon_{1c} = \varepsilon_r + \frac{\sigma_a \Delta N/\epsilon_0}{\omega^2 + i\Delta\omega_a\omega - \omega_a^2}, \qquad \Delta N \approx \frac{\tau R_\mathrm{p}}{1+\tau R_\mathrm{p}}\overline{N}_0, \tag{A4}$$

where ε_r is the relative permittivity of the core's host dielectric, σ_a is a constant determining the active molecule coupling to electric fields, ω_a is the emission angular frequency, and $\Delta\omega_a$ is the bandwidth. The second equation in Eq. (A4) represents the approximate population difference ΔN between the lasing energy states, in which $\overline{N}_0$ is the total active dye concentration, τ is the lifetime of the radiative transition, and R_p is the pump rate. In the example in Sec. V, for the gold Drude model, we assume $\varepsilon_\infty = 9.5$, $\omega_p = 1.36 \times 10^{16}$ rad/s, and $\Gamma = 1.05 \times 10^{14}$ s^{-1}. For the core of the active nanoparticle (silica doped with Rhodamine 6G), we assume the same parameters used in Ref. [56] (adapted from experimental data [82,78]): $\varepsilon_r = 2.25$, $\sigma_a = 6.55 \times 10^{-8}$ C^2/kg, $f_a = \omega_a/(2\pi) = 526$ THz, $\tau = 4$ ns, $\overline{N}_0 = 3 \times 10^{18}$ cm^{-3}, $R_p = 3 \times 10^9$ s^{-1}, and $\beta = (r_{1c}/r_{1s})^3 = 0.9$. The polarizabilities of the two particles at the EPD frequency of 520 THz when $r_{1s} = 26$ nm are $\alpha_2 = (2.04 + i9.87) \times 10^{-35}$ Cm^2 V^{-2} for the gold nanosphere with $r_2 = 20$ nm, and $\alpha_1 = (3.33 - i\,9.22) \times 10^{-35}$ Cm^2 V^{-2} for the active nanoshell.

[1] T. Kato, *Perturbation Theory for Linear Operators* (Springer-Verlag, Berlin Heidelberg, 1995).
[2] C. M. Bender and S. Boettcher, Phys. Rev. Lett. **80**, 5243 (1998).
[3] W. D. Heiss, M. Müller, and I. Rotter, Phys. Rev. E **58**, 2894 (1998).
[4] W. D. Heiss, J. Phys. Math. Gen. **37**, 2455 (2004).
[5] A. Figotin and I. Vitebskiy, Phys. Rev. E **74**, 066613 (2006).
[6] R. El-Ganainy, M. Khajavikhan, and L. Ge, Phys. Rev. A **90**, 013802 (2014).
[7] B. Zhen, C. W. Hsu, Y. Igarashi, L. Lu, I. Kaminer, A. Pick, S.-L. Chua, J. D. Joannopoulos, and M. Soljačić, Nature **525**, 354 (2015).

[8] J. D. Joannopoulos, S. G. Johnson, J. N. Winn, and R. D. Meade, *Photonic Crystals: Molding the Flow of Light* (Princeton University Press, Princeton, NJ, 2011).

[9] J. M. Bendickson, J. P. Dowling, and M. Scalora, Phys. Rev. E **53**, 4107 (1996).

[10] A. Figotin and I. Vitebskiy, Phys. Rev. B **67**, 165210 (2003).

[11] M. B. Stephanson, K. Sertel, and J. L. Volakis, IEEE Microw. Wirel. Compon. Lett. **18**, 305 (2008).

[12] A. Figotin and I. Vitebskiy, Phys. Rev. E **72**, 036619 (2005).

[13] J. L. Volakis and K. Sertel, Proc. IEEE **99**, 1732 (2011).

[14] N. Gutman, A. A. Sukhorukov, F. Eilenberger, and C. M. de Sterke, Opt. Express **20**, 27363 (2012).

[15] M. G. Wood, J. R. Burr, and R. M. Reano, Opt. Lett. **40**, 2493 (2015).

[16] M. A. K. Othman, F. Yazdi, A. Figotin, and F. Capolino, Phys. Rev. B **93**, 024301 (2016).

[17] V. A. Tamma, A. Figotin, and F. Capolino, IEEE Trans. Microw. Theory Tech. **64**, 742 (2016).

[18] N. Apaydin, L. Zhang, K. Sertel, and J. L. Volakis, IEEE Trans. Microw. Theory Tech. **60**, 1513 (2012).

[19] A. A. Sukhorukov, C. J. Handmer, C. M. de Sterke, and M. J. Steel, Opt. Express **15**, 17954 (2007).

[20] S. Yarga, K. Sertel, and J. L. Volakis, IEEE Trans. Antennas Propag. **57**, 799 (2009).

[21] J. R. Burr, N. Gutman, C. M. de Sterke, I. Vitebskiy, and R. M. Reano, Opt. Express **21**, 8736 (2013).

[22] M. A. Othman, M. Veysi, A. Figotin, and F. Capolino, Phys. Plasmas **23**, 033112 (2016).

[23] H. Noh, J.-K. Yang, I. Vitebskiy, A. Figotin, and H. Cao, Phys. Rev. A **82**, 013801 (2010).

[24] M. Othman and F. Capolino, IEEE Microw. Wirel. Compon. Lett. **25**, 700 (2015).

[25] M. A. Othman, M. Veysi, A. Figotin, and F. Capolino, IEEE Trans. Plasma Sci. **44**, 918 (2016).

[26] J. Sloan, M. A. K. Othman, and F. Capolino, arXiv:1609.00044.

[27] D. Oshmarin, F. Yazdi, M. A. K. Othman, J. Sloan, M. Radfar, M. Green, and F. Capolino, arXiv:1610.00415.

[28] M. Othman, V. A. Tamma, and F. Capolino, IEEE Trans. Plasma Sci. **44**, 594 (2016).

[29] R. El-Ganainy, K. G. Makris, D. N. Christodoulides, and Z. H. Musslimani, Opt. Lett. **32**, 2632 (2007).

[30] C. E. Rüter, K. G. Makris, R. El-Ganainy, D. N. Christodoulides, M. Segev, and D. Kip, Nat. Phys. **6**, 192 (2010).

[31] A. Mostafazadeh, J. Math. Phys. **43**, 205 (2002).

[32] A. Mostafazadeh, J. Math. Phys. **43**, 2814 (2002).

[33] A. Mostafazadeh, J. Phys. Math. Gen. **36**, 7081 (2003).

[34] N. Read and D. Green, Phys. Rev. B **61**, 10267 (2000).

[35] P. Cejnar, S. Heinze, and M. Macek, Phys. Rev. Lett. **99**, 100601 (2007).

[36] A. Ruschhaupt, F. Delgado, and J. G. Muga, J. Phys. Math. Gen. **38**, L171 (2005).

[37] I. V. Barashenkov, L. Baker, and N. V. Alexeeva, Phys. Rev. A **87**, 033819 (2013).

[38] G. Castaldi, S. Savoia, V. Galdi, A. Alù, and N. Engheta, Phys. Rev. Lett. **110**, 173901 (2013).

[39] A. Guo, G. J. Salamo, D. Duchesne, R. Morandotti, M. Volatier-Ravat, V. Aimez, G. A. Siviloglou, and D. N. Christodoulides, Phys. Rev. Lett. **103**, 093902 (2009).

[40] Z. H. Musslimani, K. G. Makris, R. El-Ganainy, and D. N. Christodoulides, Phys. Rev. Lett. **100**, 030402 (2008).

[41] M. Kulishov and B. Kress, Opt. Express **21**, 22327 (2013).

[42] K. G. Makris, R. El-Ganainy, D. N. Christodoulides, and Z. H. Musslimani, Phys. Rev. Lett. **100**, 103904 (2008).

[43] S. Longhi, Phys. Rev. A **82**, 031801(R) (2010).

[44] L. Ge, Y. D. Chong, S. Rotter, H. E. Türeci, and A. D. Stone, Phys. Rev. A **84**, 023820 (2011).

[45] L. Feng, Z. J. Wong, R.-M. Ma, Y. Wang, and X. Zhang, Science **346**, 972 (2014).

[46] H. Ramezani, T. Kottos, R. El-Ganainy, and D. N. Christodoulides, Phys. Rev. A **82**, 043803 (2010).

[47] Z. Lin, H. Ramezani, T. Eichelkraut, T. Kottos, H. Cao, and D. N. Christodoulides, Phys. Rev. Lett. **106**, 213901 (2011).

[48] N. Lazarides and G. P. Tsironis, Phys. Rev. Lett. **110**, 053901 (2013).

[49] M. Kang, F. Liu, and J. Li, Phys. Rev. A **87**, 053824 (2013).

[50] O. Vázquez-Candanedo, J. C. Hernández-Herrejón, F. M. Izrailev, and D. N. Christodoulides, Phys. Rev. A **89**, 013832 (2014).

[51] A. Regensburger, C. Bersch, M.-A. Miri, G. Onishchukov, D. N. Christodoulides, and U. Peschel, Nature **488**, 167 (2012).

[52] E. Lidorikis, M. M. Sigalas, E. N. Economou, and C. M. Soukoulis, Phys. Rev. Lett. **81**, 1405 (1998).

[53] M. Bayindir, B. Temelkuran, and E. Ozbay, Phys. Rev. Lett. **84**, 2140 (2000).

[54] M. H. Teimourpour, R. El-Ganainy, A. Eisfeld, A. Szameit, and D. N. Christodoulides, Phys. Rev. A **90**, 053817 (2014).

[55] Y. Jin and X. Gao, Nat. Nanotechnol. **4**, 571 (2009).

[56] S. Campione, M. Albani, and F. Capolino, Opt. Mater. Express **1**, 1077 (2011).

[57] J. D. Jackson, *Classical Electrodynamics* (John Wiley & Sons, Inc., New York, 1999), pp. 450-490.

[58] J. G. Van Bladel, *Electromagnetic Fields* (John Wiley & Sons, 2007), pp. 293-310.

[59] F. Capolino, D. R. Wilton, and W. A. Johnson, in *IEEE Antennas Propag. Soc. Int. Symp* (Albuquerque, NM, 2006), pp. 2847-2850.

[60] F. Capolino, D. R. Wilton, and W. A. Johnson, IEEE Trans. Antennas Propag. **53**, 2977 (2005).

[61] F. Capolino, D. R. Wilton, and W. A. Johnson, J. Comput. Phys. **223**, 250 (2007).

[62] S. Campione, S. Steshenko, and F. Capolino, Opt. Express **19**, 18345 (2011).

[63] C. Kittel and P. McEuen, *Introduction to Solid State Physics* (Wiley, New York, 1986).

[64] S. V. Dmitriev, A. A. Sukhorukov, and Y. S. Kivshar, Opt. Lett. **35**, 2976 (2010).

[65] S. V. Suchkov, B. A. Malomed, S. V. Dmitriev, and Y. S. Kivshar, Phys. Rev. E **84**, 046609 (2011).

[66] R. E. Collin, *Field Theory of Guided Waves* (McGraw-Hill, New York, 1960).

[67] J. J. Sakurai and J. Napolitano, *Modern Quantum Mechanics* (Addison-Wesley, Boston, 2011).

[68] A. Figotin and I. Vitebskiy, Phys. Rev. E **68**, 036609 (2003).

[69] D. S. Bethune, J. Opt. Soc. Am. B **6**, 910 (1989).

[70] A. Figotin and I. Vitebskiy, Waves Random Complex Media **16**, 293 (2006).

[71] J. Gear, F. Liu, S. T. Chu, S. Rotter, and J. Li, Phys. Rev. A **91**, 033825 (2015).

[72] M. A. K. Othman and F. Capolino, arXiv:1610.00413.
[73] A. Welters, SIAM J. Matrix Anal. Appl. **32**, 1 (2011).
[74] J. Wiersig, Phys. Rev. A **93**, 033809 (2016).
[75] S. N. Ghosh and Y. D. Chong, Sci. Rep. **6**, 19837 (2016).
[76] Y. Li, X. Guo, L. Chen, C. Xu, J. Yang, X. Jiang, and M. Wang, J. Light. Technol. **31**, 2477 (2013).
[77] A. E. Siegman, *Lasers* (University Science Books, Mill Valley, 1986).
[78] D. Magde, R. Wong, and P. G. Seybold, Photochem. Photobiol. **75**, 327 (2002).
[79] F. Capolino, *Theory and Phenomena of Metamaterials* (CRC Press, Boca Raton, 2009).
[80] K. F. Renk, *Basics of Laser Physics: For Students of Science and Engineering* (Springer Science and Business Media, New York, 2012).
[81] D. Faubert, S. L. Chin, M. Cormier, and M. Boloten, Can. J. Phys. **57**, 160 (1979).
[82] M. A. Alencar, G. S. Maciel, C. B. de Araujo, R. Bertholdo, Y. Messaddeq, and S. J. Ribeiro, J. Non-Cryst. Solids **351**, 1846 (2005).